optica

Far-field linear optical superresolution via heterodyne detection in a higher-order local oscillator mode

FAN YANG,[1] ARINA TASHCHILINA,[1] E. S. MOISEEV,[1] CHRISTOPH SIMON,[1] AND A. I. LVOVSKY[1,2,*]

[1]Department of Physics and Astronomy, University of Calgary, Calgary T2N 1N4, Canada
[2]Russian Quantum Center, 100 Novaya St., Skolkovo, Moscow Region 143025, Russia
*Corresponding author: trekut@gmail.com

The Rayleigh limit has so far applied to all microscopy techniques that rely on linear optical interaction and detection in the far field. Here we demonstrate that detecting the light emitted by an object in higher-order transverse electromagnetic modes (TEMs) can help in achieving sub-Rayleigh precision for a variety of microscopy-related tasks. Using optical heterodyne detection in TEM_{01}, we measure the position of coherently and incoherently emitting objects to within 0.0015 and 0.012 of the Rayleigh limit, respectively, and determine the distance between two incoherently emitting objects positioned within 0.28 of the Rayleigh limit with a precision of 0.019 of the Rayleigh limit. Heterodyne detection in multiple higher-order TEMs enables full imaging with a resolution significantly below the Rayleigh limit in a way that is reminiscent of quantum tomography of optical states.   © 2016 Optical Society of America

1. INTRODUCTION

Since the invention of the optical microscope, there has been a quest for enhancing its resolution. The Rayleigh criterion [1] establishes the minimum resolvable distance in a direct image of a pair of sources to be limited by diffraction according to $d_R = 1.22\lambda/2$ NA, where λ is the wavelength and NA is the numerical aperture of the objective lens [Fig. 1(a)]. In the past century, a number of techniques for circumventing the Rayleigh limit have emerged [2]. These methods rely, for example, on using shorter-wavelength radiation [3], near-field probing [4], or nonclassical [5] or nonlinear [6] optical properties of the object or switching the object's emission on and off [7–9]. However, these approaches are often expensive and not universally applicable. Therefore, finding a linear optical microscopy technique that is operational in the far-field regime remains an important outstanding problem.

A promising approach to addressing this problem is by detecting the light emitted by the object in higher-order transverse electromagnetic modes (TEMs). A point source emits primarily into the fundamental TEM_{00} mode. However, when the emitter is displaced from the center of the fundamental mode, higher-order TEMs are illuminated. In this way, null measurements of small displacements are possible. For example, homodyne detection in TEM_{01} has been proposed for detecting small displacements of a laser beam [10] implemented for tracking particles with a nanometer resolution [11]. These experiments were performed for single emitters only.

More recently, Tsang and colleagues showed theoretically that sub-Rayleigh distances between two identical point sources can be estimated by measuring the photon count rate in TEM_{01} [12,13]. Remarkably, for distances below the Rayleigh limit, the per-photon uncertainty of this measurement is much less than that associated with direct imaging. This feature is particularly valuable when the number of photons the object can radiate is limited, such as in the case of photobleaching.

Inspired by these developments, we overcome the Rayleigh limit by means of heterodyne detection [Fig. 1(b)], taking advantage of the fact that the heterodyne detector is only sensitive to the electromagnetic field in the mode of the local oscillator (LO) [14]. We apply the technique in a variety of settings. First, we determine the positions of single objects emitting coherent and incoherent light. Second, we determine the distance between two identical incoherent objects separated by a distance below the Rayleigh limit. In both cases, we demonstrate a measurement precision significantly below that limit.

In addition, we utilize a mathematical analogy between decomposing an image into TEMs and representing the quantum state of a harmonic oscillator in the Fock basis to propose a new (to our knowledge) microscopy technique. By measuring the intensity and phase of the object's emission into all TEMs, one can completely reconstruct its image, in principle with an arbitrarily high precision. In an experiment, the imaging resolution depends on the number of TEMs in which the detection can be realized.
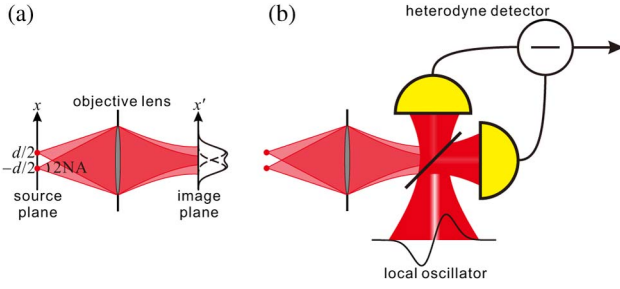
Fig. 1. Concept of the experiment. (a) Imaging with an objective lens with a finite NA leads to diffraction-limited resolution; (b) heterodyne detection of the image with the local oscillator in TEM_{01} overcomes the diffraction limit, because the detector output is nonzero only for spatially separated sources.

2. CONCEPT

Consider an optical microscope objective lens that is used to image a plane object with a transverse spatial field distribution $E(x)$. The field distribution in the image plane is then given by the convolution

$$E'(x') = \int_{-\infty}^{+\infty} E(x) T(x' - x) \, dx, \tag{1}$$

where $T(\cdot)$ is the transfer function of the objective lens and we have assumed the magnification to be unity for convenience (see Supplement 1). The transfer function can be approximated by a Gaussian

$$T(x) \approx \frac{1}{(2\pi)^{1/4} \sqrt{\sigma}} e^{-x^2/4\sigma^2}, \tag{2}$$

with the width $\sigma \approx 0.21 \lambda / \text{NA}$ [15]. The narrower the aperture in the lens, the wider the transfer function, and the stronger the distortion of the image.

The heterodyne detector generates a current that is proportional to the overlap between the LO and the signal field,

$$J \propto \int_{-\infty}^{+\infty} E'(x') E_{\text{LO}}^*(x') \, dx', \tag{3}$$

where $E_{\text{LO}}(x')$ is the spatial profile of the LO. The LO is prepared in the TEM_{01} mode such that the corresponding fundamental TEM_{00} mode is matched to the image of a point source located at $x = 0$: $E_{\text{LO}}(x') \propto \frac{1}{(2\pi)^{1/4} \sigma^{3/2}} x' e^{-x'^2/4\sigma^2}$.

For this conceptual discussion, we assume that the source is a point located at position x_p, so that $E(x) \propto \delta(x - x_p)$, in which case we have

$$J_p(x_p) \propto \int_{-\infty}^{+\infty} T(x' - x_p) E_{\text{LO}}^*(x') \, dx', \tag{4}$$

which for a Gaussian transfer function reduces to $J_p(x_p) \propto \frac{1}{2\sigma} x_p e^{-x_p^2/8\sigma^2}$, and the corresponding electronic power

$$P(x_p) \propto J_p^2(x_p) \propto \frac{1}{4\sigma^2} x_p^2 e^{-x_p^2/4\sigma^2}. \tag{5}$$

The signal vanishes at $x_p = 0$, enabling sensitive null measurement of the source position with respect to the central point [10].

Especially useful is the enhancement associated with determining the distance d between two incoherent point sources. Suppose the sources are located at $x = \pm d/2$, where d is the distance between them. The signal in TEM_{01} is given by

$P(d/2) + P(-d/2)$, which is proportional to d^2 in the leading order. The intensity in the direct image of this object, on the other hand, is given by $I(x') \propto S(x' + d/2) + S(x' - d/2)$, where $S(\cdot) = |T(\cdot)|^2$ is the point spread function of the microscope. Approximating $S(x' \pm d/2) = S(x') \pm \frac{d}{2} \frac{\partial}{\partial x} S(x') + O(d^2)$, we find $I(x') \propto 2S(x') + O(d^2)$. The effect on the image due to the separation of the slits is also of the second order in d, but with a macroscopic zeroth-order background. Any noise in this background will have a deleterious effect on the measurement precision of the term of interest.

3. EXPERIMENT

The experimental setup is shown in Fig. 2. Both the signal and LO are obtained from a homemade external cavity diode laser, producing $\sim$45 mW at a wavelength of $\lambda = 780$ nm. We prepare the LO in the desired TEM by transmitting it through a temperature-stabilized monolithic cavity with a finesse of about 275 [16]. The laser frequency is locked to the cavity resonance by means of the Pound–Drever–Hall technique [17]. The signal beam passes through an acousto-optic modulator operating at 40 MHz. In this way, our setup implements heterodyne, rather than homodyne, detection, which helps reduce the flicker noise at low electronic frequencies. The modulated beam is collimated to about a 5 mm diameter and sent to a diaphragm with four pairs of slits of 0.15 mm width whose centers are separated by $d = 0.25$, 0.50, 0.75, and 1.00 mm (3B Scientific U14101). The power of the beam transmitted through the slits is $\sim$200 µW. For the measurements with incoherent light, we place a white paper library card before the slits. During the data acquisition, the card is moved in the transverse plane by a motorized translation stage to achieve averaging over the incoherent light statistics. The incoherent optical power behind the slits is $\sim$10 µW. After the slits, the light propagates in free space for $L = 84$ cm and passes through an iris diaphragm. The diameter of the diaphragm is measured using an optical microscope as 0.8 ± 0.1 mm and independently estimated with a higher precision from the fit to the data as 0.87 ± 0.01 mm. This latter value corresponds to NA = 0.52×10^{-3} and a Rayleigh distance of $d_R = 0.912$ mm.

The field transmitted through the diaphragm is refocused by an objective lens and subjected to heterodyne detection by means of a balanced detector (ThorLabs PDB150A-SP). To align the detector, we first match the signal's mode to the LO prepared in TEM_{00}. Subsequently, the monolithic cavity temperature is changed to transmit the TEM_{01} mode, and the LO is adjusted
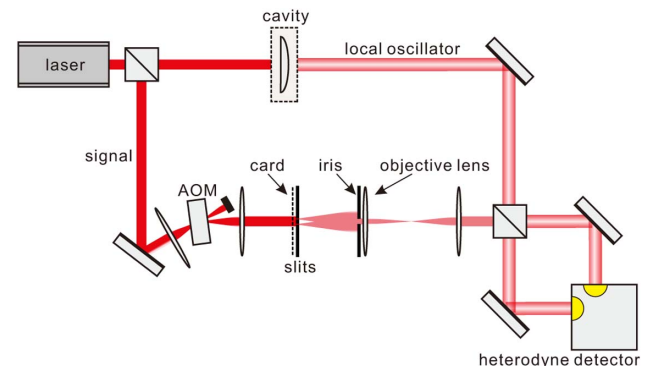

Fig. 2. Experimental setup. AOM, acousto-optic modulator.

slightly to minimize the interference with the signal. The output photocurrent from that detector is observed with a spectrum analyzer set to a zero span mode at 40 MHz with a resolution bandwidth of 1 kHz and a video bandwidth of 10 kHz. An average of 100 traces are acquired for each measurement.

4. RESULTS AND DISCUSSION

We first measure the position of a single light source. In this case, the beam only passes through a single 0.15 mm slit, whose position x_p is controlled by a translation stage. We conduct the measurement for both coherent and incoherent light.

In the coherent case, our setting resembles that proposed by Hsu *et al.* [10]. We acquire the data for each point in Fig. 3(a) once, except for a set of points around $x_p = 0$ shown in the inset. For these latter points, the signal value is acquired 10 times to estimate the stochastic experimental error. Two types of experimental imperfections contribute to that error. First, the orthogonality between the LO and signal modes is imperfect and fluctuates due to air movements and vibration of the optics. As a result, the magnitude of the signal power fluctuation at $x_p = 0$ is comparable to the signal itself. Second, the power of the LO fluctuates due to the instability of the lock of the laser to the cavity resonance. These fluctuations translate directly into those in the detector's output, so the errors at high signals are proportional to the signal.
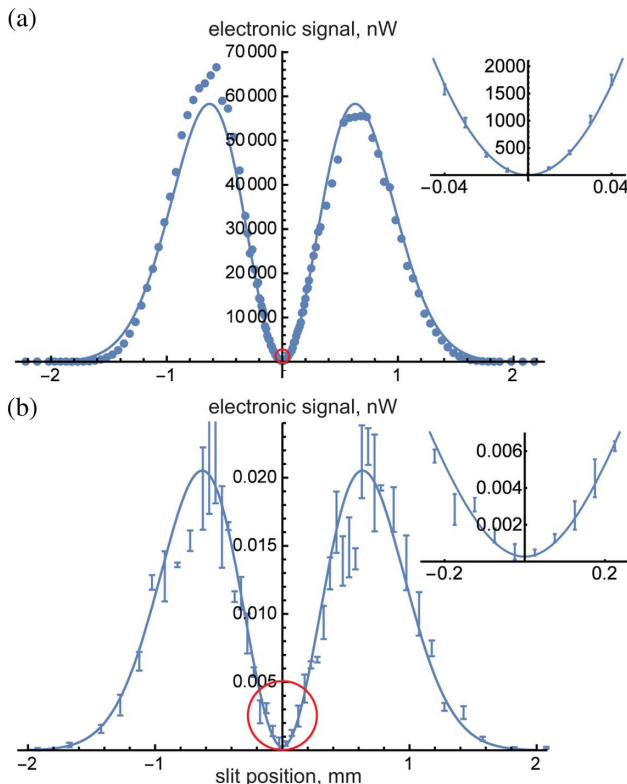

(a)

(b)

Fig. 3. Single-slit positioning experiment. The dependence of the heterodyne detector output signal on the slit position measured (a) with coherent light and (b) with incoherent light is displayed. The theoretical predictions take into account the finite width of the slit, but are largely similar to those of Eq. (5) (see Supplement 1). The theory is fit to the experimental data by varying the vertical scale and diaphragm diameter. The insets show the areas around the origin, approximately corresponding to the red circles in the corresponding main plots, magnified.

In view of this analysis, we model the error of our measurement to behave as $\Delta^2 = c^2 + (gP)^2$, where c is the uncertainty due to the mode mismatch fluctuations and gP is due to the fluctuations of the LO. The actual experimental behavior of the error is consistent with this model. We use this model to find the uncertainty of estimating the slit position x_p from the signal power. To this end, we calculate the Fisher information as a function of x_p and find that this function is maximized at $x_p = 0.012$ mm. The value of the Fisher information at this point corresponds to a Cramér–Rao uncertainty bound [18] of $\delta x_p = 1.4$ μm, almost three orders of magnitude below the Rayleigh limit (see Supplement 1).

In the experiment with incoherent light [Fig. 3(b)], the signal's spatial structure is a speckle pattern, changing in time as we move the library card. The intensity of the signal field in the mode being detected is then governed by thermal statistics, so large fluctuations, whose magnitude is on the scale of the signal, are present even for large signals. While the effect of these fluctuations is reduced due to averaging, it is still the dominant source of error for high signal powers. For low signal powers, similar to the coherent case, the contribution to the uncertainty associated with nonconstant mode matching between the signal and LO becomes significant. The general behavior of the experimental error is therefore still consistent with $\Delta^2 = c^2 + (gP)^2$, albeit with different values of c and g compared to the coherent case. Experimentally, we evaluate these coefficients by acquiring the heterodyne signal at each x_p three times. We find that the Fisher information is maximized and the uncertainty of x_p is minimized for $x_p = 0.14$ mm, corresponding to $\delta x_p = 11$ μm.

Next, we measure the distance between two incoherent light sources. Each slit pair is centered on the laser beam, and the output signal is sampled 12 times to estimate the error. The resulting data are shown in Fig. 4(b). The error analysis for this setting is similar to that for a single incoherent slit and yields a minimum of $\delta d = 17$ μm for $d = 0.18$ mm.

It is interesting to compare the precision of our measurement with what can be achieved by conventional imaging. The images of pairs of slits acquired with a conventional CCD camera are shown in Fig. 4(a), bottom row. For separations significantly below the Rayleigh limit, these images do not resolve the slits and cannot be used to determine the separations. Our technique, on the other hand, permits this determination with precision comparable to the camera pixel size (7 μm).

At a more quantitative level, the above error analysis implies that the Fisher information decreases to zero, and the estimation uncertainty tends to infinity, for $d \to 0$. This is a common feature of both our technique and conventional imaging, arising because of a nonvanishing uncertainty in evaluating the signal at $d = 0$ (see Supplement 1). The fundamental reason for this feature in both cases is the shot noise. In practice, the limitation in our experiment is the fluctuation of the mode matching between the LO and the signal, which can be reduced by using more stable optics. Furthermore, the shot noise level can be reduced by using squeezing [10,11]. The conventional imaging technique, on the other hand, is often limited by technical fluctuations of the electronic signal produced by individual pixels in the camera, which complicates precise measurement of minute image width variations associated with varying d. Note that the techniques of Refs. [12,13] utilize photon counting in higher-order modes and do not suffer from the fundamental precision limitation
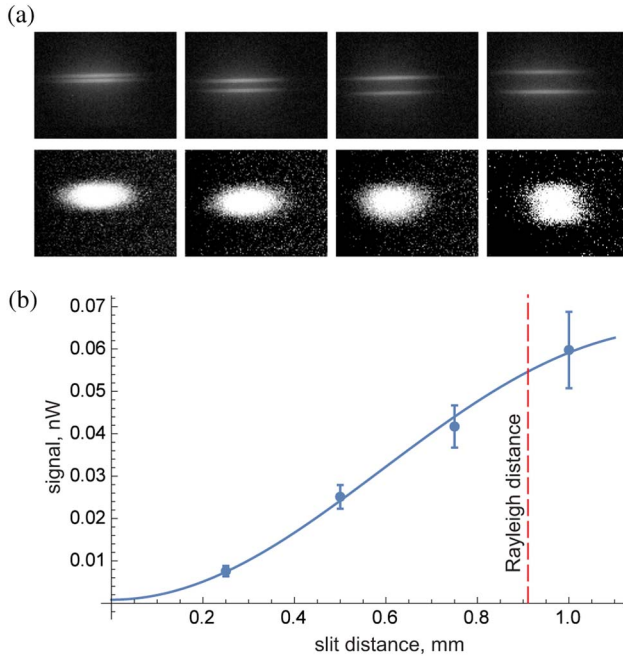
(a)

(b)

Fig. 4. Incoherent double slit experiment. (a) Images of the slits with the iris diaphragm fully open (top row) and closed to a 0.8 mm diameter (bottom row) for $d = 0.25$, 0.50, 0.75, and 1.00 mm, left to right. The slits with $d < 1.00$ mm are not resolved with the closed diaphragm setting. (b) Dependence of the signal in TEM_{01} on the slit distance. The error bars show the statistical errors of 12 measurements each.

associated with the shot noise. These methods are, however, still vulnerable to practical noise sources such as detector dark counts.

5. APPLICATION TO IMAGING

Heterodyne detection in TEM_{01} can estimate the distance between two light sources, but only if it is known *a priori* that the source consists of two identical points. However, performing this measurement also in higher-order Hermite–Gaussian modes permits reconstruction of the full image of an object with sub-Rayleigh resolution. Here we show this for the one-dimensional case; the extension to two dimensions is straightforward.

We write the heterodyne detector output photocurrent [Eq. (3)] as

$$J_{0n} \propto \int_{-\infty}^{+\infty} E(x)J(x)\mathrm{d}x, \tag{6}$$

where $J(x)$ is the photocurrent in response to a point source at x given by Eq. (4). We assume, as previously, that the transfer function is given by Eq. (2), while the LO is in TEM_{0n} of width σ:

$$E_{\mathrm{LO},n}(x) \propto \frac{H_n(x/\sqrt{2}\sigma)}{(2\pi)^{1/4}\sqrt{2^n n!}\sigma}e^{-x^2/4\sigma^2}, \tag{7}$$

where $H_n(\cdot)$ represents the Hermite polynomials. The integral [Eq. (4)] then corresponds to a Weierstrass transform of that polynomial, and is given by a remarkably simple expression:

$$J_{p,0n}(x) \propto \frac{1}{\sqrt{n!}}\left(\frac{x}{2\sigma}\right)^n e^{-x^2/8\sigma^2}. \tag{8}$$

We see that for objects of size $\lesssim \sigma$, photocurrent J_{0n} gives the nth moment of the field in the object plane.

The set of photocurrents acquired for multiple modes can be further utilized to find the decomposition of $E(x)$ into the Hermite–Gaussian basis and thereby reconstruct the full image of the object with a sub-Rayleigh resolution. Let α_{kn} be the coefficients of the Hermite polynomial of degree k, so that $H_k(x/2\sigma) = \Sigma_n \alpha_{kn}(x/2\sigma)^n$. Then, according to Eqs. (6) and (8), we have

$$\beta_k := \sum_n \sqrt{n!}\,\alpha_{kn}J_{0n} = \int_{-\infty}^{+\infty} E(x)H_k\left(\frac{x}{2\sigma}\right)e^{-x^2/8\sigma^2}\mathrm{d}x. \tag{9}$$

Because Hermite–Gaussian functions form an orthonormal basis in the Hilbert space of one-dimensional functions, it follows that

$$E(x) \propto \sum_{k=0}^{\infty} \frac{\beta_k H_k(x/2\sigma)e^{-x^2/8\sigma^2}}{2^{k+1}k!\sqrt{\pi}\sigma}. \tag{10}$$

Knowing all values of β_k, we can calculate $E(x)$. This approach is reminiscent of representing a quantum state of a harmonic oscillator as a superposition of Fock states, whose wave functions in the position basis are given by Hermite–Gaussian functions.

We name the above-described imaging technique Hermite–Gaussian microscopy, or HGM. Acquiring heterodyne photocurrents for a sufficiently high number of TEMs in principle allows HGM to reconstruct the image with arbitrarily high resolution. The first few tens of TEMs, which are attainable in experimental optics, permit significant improvement in imaging with respect to the Rayleigh limit, as evidenced in Fig. 5.
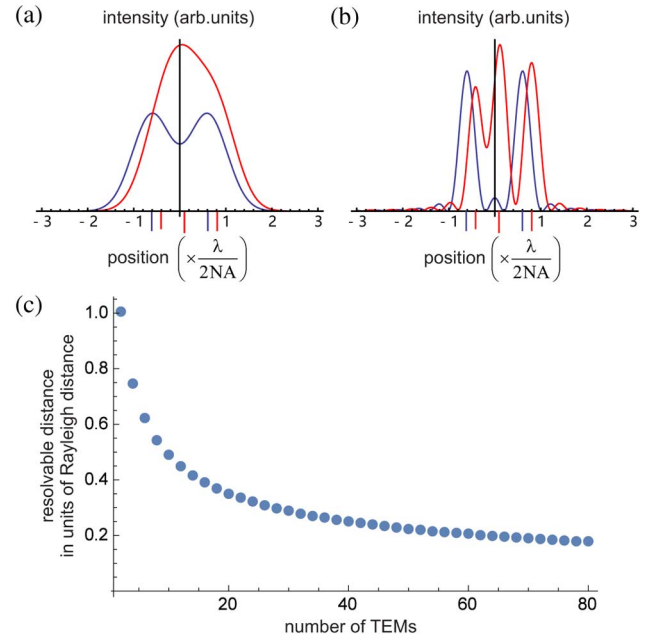
(a)

(b)

(c)

Fig. 5. Hermite–Gaussian microscopy. (a) Expected images with conventional imaging. Blue curve: an image of two single sources positioned at $1.22\lambda/2\,\mathrm{NA}$, which corresponds to the Rayleigh limit. Red curve: an image of three slits with different intensities positioned at distances below Rayleigh limit. The positions and relative intensities of the sources are shown below the abscissa axis. (b) Images of the same objects expected in HGM with TEM_{0n} for $0 \leq n \leq 20$ exhibiting triple enhancement of resolution. (c) Resolution of HGM, in units of the Rayleigh distance $1.22\lambda/2\,\mathrm{NA}$, as a function of the number of TEMs used. The resolution is defined as the minimum distance between the point objects such that the image intensity at the center does not exceed 75% of the maximum intensity.

The above conceptual description can be readily extended to practically relevant cases. Two-dimensional imaging is possible by scanning over both indices of TEM_{mn} and measuring the photocurrent J_{mn} for each pair (m, n) up to a desired maximum. Acquiring both the sine and cosine quadratures of the heterodyne photocurrent permits phase-sensitive reconstruction of the object's field.

A somewhat less trivial extension is to incoherent images. In this case, the output power of the heterodyne detector is given by

$$\langle P_{0n} \rangle \propto \frac{1}{n!} \int_{-\infty}^{+\infty} I(x) \left(\frac{x}{2\sigma} \right)^{2n} e^{-x^2/4\sigma^2} \qquad \textbf{(11)}$$

(see Supplement 1 for the derivation). Similar to the coherent case, we obtain moments of the field distribution in the object plane. However, now we obtain only the even coefficients of the decomposition of $I(x)$ into the Hermite–Gaussian basis. Therefore, the information about only the even component of function $I(x)$ is retained. An image reconstructed with these data will be a sum of the original intensity profile $I(x)$ with the collateral image $I(-x)$. For two-dimensional microscopy, three collateral images, $I(x, -y)$, $I(-x, y)$, and $I(-x, -y)$, will be added to the original image $I(x, y)$. Their effect can be eliminated by placing the entire object in a single quadrant of the x–y plane.

6. SUMMARY

We have used heterodyne detection in the TEM_{01} Hermite–Gaussian mode to obtain sub-Rayleigh precision in the measurement of the position of single coherent and incoherent sources, as well as that of the separation between two incoherent sources. With numerical apertures below 10^{-3}, our measurement precision is on a scale of a few micrometers. If our technique is used with state-of-the-art microscopes with NA ~ 1, precision on nanometer scales can be expected. By utilizing higher Hermite–Gaussian modes, the technique can be extended to full imaging with sub-Rayleigh resolution.

Although our report demonstrates the practicality of heterodyne detection in a higher-order local oscillator mode for super-resolution microscopy, we do not quantify the advantage with respect to direct imaging in terms of per-photon Fisher information, as is done in Ref. [12] for direct photon detection in TEM_{01}. If the shot noise is the only noise source, our technique may be advantageous in measuring the distance between incoherent point sources, but this is unlikely to be the case for measuring the position of a coherent or incoherent single source. A study of this question will be presented in a separate publication. Another important question is the application of our method to estimating the separation of a coherently illuminated pair of sources. In this case, the signal depends on the relative phase between them. If the sources are in phase, the field distribution in the image plane is an even function and hence contains no component in TEM_{01}, so a nonzero signal can be expected only in TEM_{02} and higher even TEMs. If, however, the phases are shifted with respect to each other, a nonvanishing signal in TEM_{01} will be observed. Again, we are deferring a quantitative comparison of this method's precision with that of direct imaging to a future study.

See Supplement 1 for supporting content.

REFERENCES

1. E. Hecht, *Optics* (Addison-Wesley, 2002).
2. S. W. Hell, "Far-field optical nanoscopy," Science **316**, 1153–1158 (2007).
3. A. Schropp, R. Hoppe, J. Patommel, D. Samberg, F. Seiboth, S. Stephan, G. Wellenreuther, G. Falkenberg, and C. G. Schroer, "Hard x-ray scanning microscopy with coherent radiation: beyond the resolution of conventional x-ray microscopes," Appl. Phys. Lett. **100**, 253112 (2012).
4. U. Durig, D. W. Pohl, and F. Rohner, "Near-field optical-scanning microscopy," J. Appl. Phys. **59**, 3318–3327 (1986).
5. V. Giovannetti, S. Lloyd, and L. Maccone, "Advances in quantum metrology," Nat. Photonics **5**, 222–229 (2011).
6. S. W. Hell and J. Wichmann, "Breaking the diffraction resolution limit by stimulated emission: stimulated-emission-depletion fluorescence microscopy," Opt. Lett. **19**, 780–782 (1994).
7. E. Betzig, G. H. Patterson, R. Sougrat, O. W. Lindwasser, S. Olenych, J. S. Bonifacino, M. W. Davidson, J. Lippincott-Schwartz, and H. F. Hess, "Imaging intracellular fluorescent proteins at nanometer resolution," Science **313**, 1642–1645 (2006).
8. M. J. Rust, M. Bates, and X. Zhuang, "Sub-diffraction-limit imaging by stochastic optical reconstruction microscopy (STORM)," Nat. Methods **3**, 793–796 (2006).
9. R. M. Dickson, A. B. Cubitt, R. Y. Tsien, and W. E. Moerner, "On/off blinking and switching behaviour of single molecules of green fluorescent protein," Nature **388**, 355–358 (1997).
10. M. T. L. Hsu, V. Delaubert, P. K. Lam, and W. P. Bowen, "Optimal optical measurement of small displacements," J. Opt. B **6**, 495–501 (2004).
11. M. A. Taylor, J. Janousek, V. Daria, J. Knittel, B. Hage, H.-A. Bachor, and W. P. Bowen, "Biological measurement beyond the quantum limit," Nat. Photonics **7**, 229–233 (2013).
12. M. Tsang, R. Nair, and X.-M. Lu, "Quantum theory of superresolution for two incoherent optical point sources," Phys. Rev. X **6**, 031033 (2016).
13. R. Nair and M. Tsang, "Interferometric superlocalization of two incoherent optical point sources," Opt. Express **24**, 3684–3701 (2016).
14. A. I. Lvovsky and M. G. Raymer, "Continuous-variable optical quantum-state tomography," Rev. Mod. Phys. **81**, 299–332 (2009).
15. B. Zhang, J. Zerubia, and J.-C. Olivo-Marin, "Gaussian approximations of fluorescence microscope point-spread function models," Appl. Opt. **46**, 1819–1829 (2007).
16. P. Palittapongarnpim, A. MacRae, and A. I. Lvovsky, "Note: a monolithic filter cavity for experiments in quantum optics," Rev. Sci. Instrum. **83**, 066101 (2012).
17. R. W. P. Drever, J. L. Hall, F. V. Kowalski, J. Hough, G. M. Ford, A. J. Munley, and H. Ward, "Laser phase and frequency stabilization using an optical resonator," Appl. Phys. B **31**, 97–105 (1983).
18. A. van den Bos, *Parameter Estimation for Scientists and Engineers* (Wiley, 2007), Chap. 4, pp. 45–97.
19. T. Z. Sheng, K. Durak, and A. Ling, "Fault-tolerant and finite-error localization for point emitters within the diffraction limit," arXiv:1605.07297 (2016).
20. W.-K. Tham, H. Ferretti, and A. M. Steinberg, "Beating Rayleigh's curse by imaging using phase information," arXiv:1606.02666 (2016).
21. M. Paur, B. Stoklasa, Z. Hradil, L. L. Sanchez-Soto, and J. Rehacek, "Achieving quantum-limited optical resolution," arXiv:1606.08332 (2016).
22. M. Tsang, "Subdiffraction incoherent optical imaging via spatial-mode demultiplexing," arXiv:1608.03211 (2016).